Angewandte International Edition Chemie

DOI: 10.1002/anie.201103341

Protein Engineering

# Protein Photoconductors and Photodiodes**

*Yuichi Tokita,* Seiji Yamada, Wei Luo, Yoshio Goto, Nicole Bouley-Ford, Hiroshi Nakajima, and Yoshihito Watanabe**

Long-range electron transfer (ET) through proteins plays important roles in living systems. ET proteins can be regarded as wide-band-gap molecular semiconductors with "dopants" (redox or photoactive species) that provide an electron- or hole-localizing site, though the protein scaffold has insulating character.[1–10] Intramolecular ET in proteins has been investigated in detail by many groups to elucidate the factors that control the rates of these nonadiabatic reactions.[1–9,11–13] Dutton and co-workers proposed a square barrier ET rate model,[11,12] while Gray and colleagues showed that ET depends on the structure of the medium between an electron donor and acceptor.[5–9]

We have investigated photoinduced ET in two proteins, zinc-substituted cytochrome $b_{562}$ (Zn-cyt $b_{562}$) and zinc-substituted cytochrome *c* (Zn-cyt *c*), the semiconductor properties of which depend on the charge distribution on their molecular surfaces: Zn-cyt $b_{562}$ has n-type semiconductor character while Zn-cyt *c* is p-type, although the active center of the two systems is virtually identical. This finding may open up the world of protein-based electronics, because the semiconductor character of proteins could be controlled by variations in surface charge.

Zn-cyt $b_{562}$ on the $H_2N$-SAM/Au electrode (SAM = self-assembled monolayer) was prepared according to the literature (see the Supporting Information). The orientation of Zn-cyt $b_{562}$ on the $H_2N$-SAM/Au surface (Figure 1) is optimal for favorable heme-region (acidic patch) electrostatic interactions with the SAM positive charge.[14]

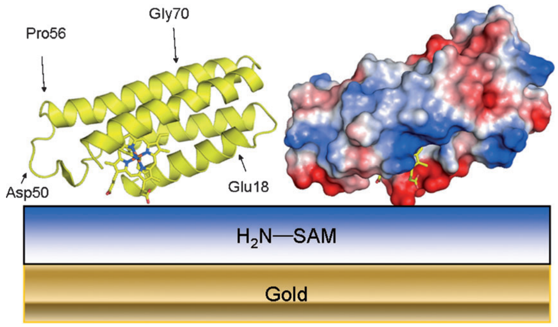


***Figure 1.*** Schematic view of Zn-cyt $b_{562}$ immobilized on $H_2N$-SAM fabricated on a gold electrode. Left: ribbon model with the porphyrin moiety in rod model; right: charge distribution of Zn-cyt $b_{562}$. Red and blue indicate negative and positive charges, respectively.

Figure 2a shows cathodic photocurrents in response to switching on and off of 420 nm illumination for bias voltages of +300, 0, and −300 mV (vs. Ag|AgCl). The action spectrum (Figure 2b) is similar to the absorption spectrum of Zn-cyt $b_{562}$ (Figure 2b, inset), which suggests that the photocurrent originates in the protein. Incidentally, there is no photocurrent response in the case that protein changes Zn-cyt $b_{562}$ into Fe-cyt $b_{562}$. Notably, the Q-band (550 nm) photocurrent response is more prominent in comparison with the absorption spectrum, that is, the Soret/Q ratio in absorbance ($I_{420}/I_{550}$) of the action spectrum is 3.7 whereas that of the UV/Vis spectrum is 11.1, thus implying that the photocurrent is derived from migration of the photoexcited electron.[15,16] These findings are consistent with this mechanism: 1) the photocurrent was observed only in the cathodic direction under the range of bias potential employed here (Figure 2c), and 2) addition of methyl viologen ($E_0 = -0.62$ V vs. Ag|AgCl) to the solution as a redox reagent enhanced the cathodic photocurrent, while addition of potassium ferri/ferrocyanide ($E_0 = +0.17$ V vs. Ag|AgCl) did not show such an effect.[17,18]

This is quite in contrast to the Zn-cyt *c*/HOOC-SAM/Au system, where the photocurrent action spectrum can be superimposed on the UV/Vis spectrum and the addition of the ferri/ferrocyanide effectively increases the photocurrent that derives from the hole in the occupied molecular orbitals (MOs), or the valence band.[13] Thus, although Zn-cyt $b_{562}$ and Zn-cyt *c* are derivatives from similar ET proteins, the systems have a different electronic nature: a photodiode (n-type) and a photoconductor (p-type) character, respectively (Figure 2c).

To elucidate the electronic structure and the factors that control the semiconductor properties of the two Zn-cytochrome proteins, we carried out all-electron DFT calculations for Zn-cyt $b_{562}$. We estimated the photoinduced ET rate constants for Zn-cyt *c* [Eq. (1)]:

$$k_{\mathrm{i}\to\mathrm{f}} = 2\pi/\hbar \times |H_{\mathrm{fi}}|^2 \delta(E_{\mathrm{fi}}) \quad (1)$$

where $H_{\mathrm{fi}}$ is the electronic coupling matrix between effective initial and final MOs, and $E_{\mathrm{fi}}$ is the corresponding orbital energy difference.[13,19]

It is noteworthy that the energy levels of MOs undergo aggregation with a band gap (ca. 2 eV) like a typical

[*] Dr. Y. Tokita, Dr. S. Yamada, W. Luo, Dr. Y. Goto, N. Bouley-Ford
Advanced Materials Laboratories, Sony Corporation
4-16-1 Okata, Atsugi-shi, Kanagawa 243-0021 (Japan)
E-mail: yuichi.tokita@jp.sony.com
yoshi@nucc.cc.nagoya-u.ac.jp
Prof. Dr. H. Nakajima, Prof. Dr. Y. Watanabe
Department of Chemistry, Graduate School of Science
Nagoya University, Furo-cho, Chikusa-ku, Nagoya 464-8602 (Japan)

[**] We thank Harry B. Gray and Jay R. Winkler (California Institute of Technology) for helpful discussions and comments.

Supporting information for this article is available on the WWW under http://dx.doi.org/10.1002/anie.201103341.

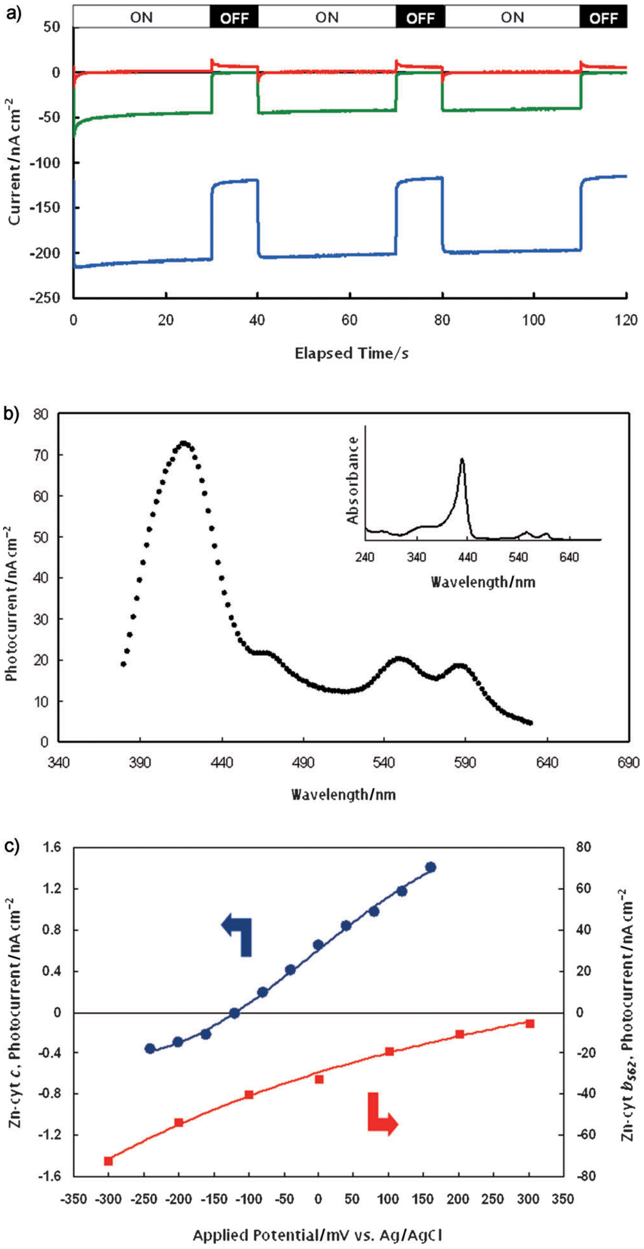


***Figure 2.*** a) Photocurrents of the Zn-cyt $b_{562}$/$H_2N$-SAM/Au electrode upon illumination at 420 nm in $N_2$-saturated 10 mM sodium phosphate buffer (pH 7.0). Applied bias potentials (vs. Ag|AgCl) are +300 (red), 0 (green), and −300 mV (blue). b) Plots of the photocurrents of the Zn-cyt $b_{562}$/$H_2N$-SAM/Au electrode in $N_2$-saturated 10 mM sodium phosphate buffer (pH 7.0). The applied potential was held at 300 mV (vs. Ag|AgCl). Inset: UV/Vis absorption spectrum of Zn-cyt $b_{562}$ in the buffer solution. c) Plots of photocurrent against applied bias potential for the Zn-cyt $b_{562}$/$H_2N$-SAM/Au (red) and Zn-cyt *c*/HOOC-SAM/Au (blue) electrodes in $N_2$-saturated 10 mM sodium phosphate buffer (pH 7.0).

semiconductor's band structure, which is also seen in previously studied cyt *c* and Zn-cyt *c* systems.[13,20] The calculated band gap (ca. 2 eV) is somewhat smaller than the estimated value from polypeptide (ca. 4 eV).[8] This might be attributed to the difference between the target sizes for estimation, polypeptide (small) and protein (large), and the effect of a DFT method that is known to underestimate the band gap.[20,21] Among the 8758 MOs, those responsible for photoexcitation of the porphyrin moiety (Gouterman's four-orbital model)[22] in Zn-cyt $b_{562}$ can be assigned to occupied MOs 3302 and 3304 having porphyrin π nature with zinc–sulfur π-bonding and unoccupied MOs 3326 and 3329 having porphyrin π* nature (Figure S2 and Table S2 in the Supporting Information), on the basis of the time-dependent DFT calculation previously obtained (Figure S3, Table S2).[13]

The intramolecular ET rate constants of photoexcited Zn-cyt $b_{562}$ were estimated from Equation (1) and related to Gouterman's 4-orbitals.[13,19,21,23] As is seen in the case of Zn-cyt *c* (Figure S5 in the Supporting Information), distinct ET rates for specific couples of MOs in Zn-cyt $b_{562}$ are observed (Figure S4). Dominant intramolecular ET rate constants for each of Gouterman's 4-orbitals of Zn-cyt $b_{562}$ and Zn-cyt *c* are summarized in Table 1. In Zn-cyt $b_{562}$, the rate constants

***Table 1:*** Calculated ET parameters for Zn-cyt $b_{562}$ and Zn-cyt *c*.

| Proteins | MO pairs | $H_{fi}$ [eV] | $E_{fi}$ [eV] | $k_{i\rightarrow f}$ [$s^{-1}$] |
|---|---|---|---|---|
| Zn-cyt $b_{562}$ | 3302_3300 | $-8.52\times10^{-1}$ | $-4.41\times10^{-2}$ | $1.57\times10^{17}$ |
| | 3304_3307 | $-6.94\times10^{-1}$ | $+1.11\times10^{-1}$ | $4.15\times10^{16}$ |
| | 3326_3325 | $-5.71\times10^{-1}$ | $-5.50\times10^{-2}$ | $5.66\times10^{16}$ |
| | 3329_3331 | $+1.15\times10^{0}$ | $+9.11\times10^{-3}$ | $1.39\times10^{18}$ |
| | 3329_3332 | $-7.33\times10^{-1}$ | $+1.48\times10^{-2}$ | $3.46\times10^{17}$ |
| Zn-cyt *c*[a] | 3268_3270 | $-3.51\times10^{-1}$ | $+2.27\times10^{-2}$ | $5.17\times10^{16}$ |
| | 3272_3271 | $-6.15\times10^{-2}$ | $-9.24\times10^{-5}$ | $3.91\times10^{17}$ |
| | 3297_3296 | $-4.91\times10^{-2}$ | $-1.59\times10^{-2}$ | $1.45\times10^{15}$ |
| | 3299_3298 | $+9.40\times10^{-2}$ | $-1.14\times10^{-1}$ | $7.42\times10^{14}$ |

[a] Reference [13].

between unoccupied MOs are one order of magnitude larger than those between the occupied MOs. The two unoccupied MOs are localized on the outermost amino acid residues around Gly70 (MO3331) and Pro56 (MO3332), respectively, which are located on the opposite side of the protein/SAM interface and exposed to the solution (Figures 1 and 3a; Figure S2 and Table S2 in the Supporting Information). On the other hand, the two occupied MOs are localized on the Glu18 (MO3300) and Asp50 (MO3307), respectively, and both reside on the electrode-contact side (Figure 1, and Figure S2 and Table S2 in the Supporting Information). Hence the major mechanism of ET in the photoexcited Zn-cyt $b_{562}$ is "ET in the conduction band" through two-state coupling between unoccupied MOs, which shows that the photoexcited Zn-cyt $b_{562}$ is an n-type semiconductor.[24] This is quite different from Zn-cyt *c*, where "hole transfer (HT) in the valence band" between occupied MOs dominates. This protein is a p-type semiconductor (Figure 2c, Table 1), even though the "dopant" is the same as in Zn-cyt $b_{562}$.

Why is one protein n-type and the other a p-type semiconductor? We analyzed the ground-state electronic structures of both proteins (Figure 3b). MO energies of Zn-cyt $b_{562}$ are generally higher than those of Zn-cyt *c*, which reflects a difference in charge of the two proteins: Zn-cyt $b_{562}$ and Zn-cyt *c* have negative (isoelectric point, pI = 5.5) and positive (pI = 9.6) charges at pH 7.0, respectively. Importantly, the effect of the negative charge of Zn-cyt $b_{562}$ on its 4-orbital energies is more prominent than that of the other porphyrin MOs assigned to porphyrin σ orbitals and the MOs localized on amino acid residues. The differences in MO

  

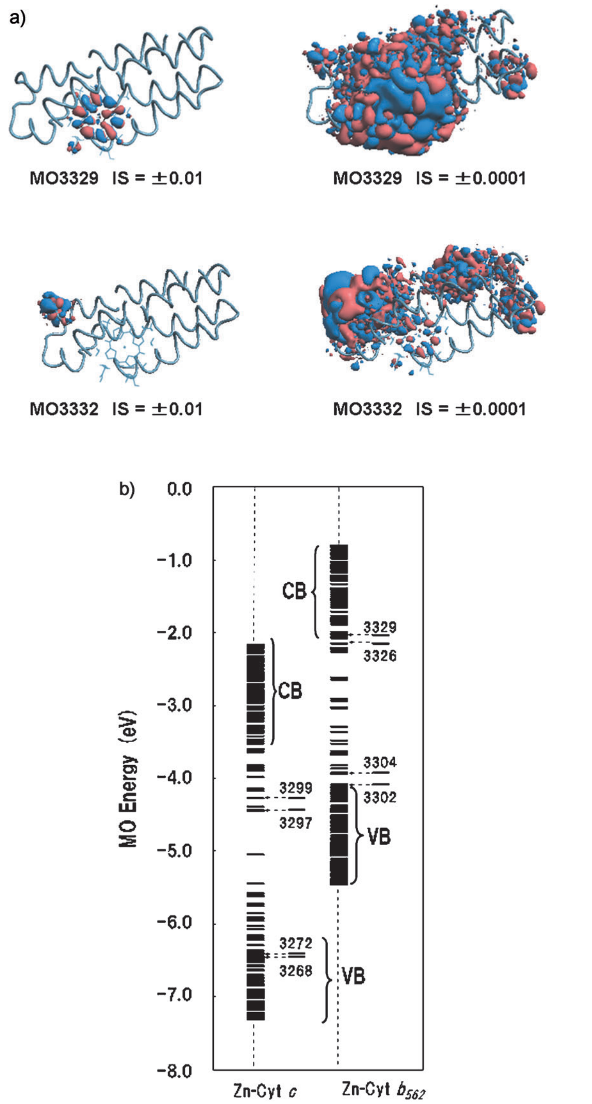


***Figure 3.*** a) Main MOs responsible for photoexcited ET in Zn-cyt $b_{562}$. MO3329 (top) has the characteristics of one of Gouterman's 4-orbitals and MO3332 (bottom) originates in the protein scaffold for which the energy level is involved in the "conduction band" of the protein and is quite close to MO3329. IS: isosurface value. b) Kohn–Sham orbital distributions around the band gap of Zn-cyt $b_{562}$ and Zn-cyt $c$. Numbers represent Gouterman's 4-orbitals of the proteins. CB: conduction band; VB: valence band. The MO3332 shown in (a) is in the CB and its energy level (−2.02 eV) is very close to that of MO3329 (−2.04 eV).

energy levels of each corresponding 4-orbital between the two systems are almost the same, +2.34 eV, although the average energy shift from Zn-cyt $c$ to Zn-cyt $b_{562}$ is +1.38 eV. Hence the relative energy level of the 4-orbitals against protein bands consisting of MOs localized on amino acid residues is very different for the two proteins. In Zn-cyt $b_{562}$, the unoccupied 4-orbitals (MOs 3326 and 3329) locate in the lower region of the protein's conduction band, whereas such an overlap is not found in Zn-cyt $c$ (Figure 3b). On the other hand, the occupied 4-orbitals (MOs 3302 and 3304) are placed at a shallow position in the higher valence band of Zn-cyt $b_{562}$. In comparison to Zn-cyt $c$, the MOs with holes and the valence band with amino acid character are more weakly coupled in Zn-cyt $b_{562}$ (Figure 3b). These electronic structure differences between the two proteins dictate the molecular-semiconductor nature of the proteins.

Why are the 4-orbitals so much more sensitive to charge than the other MOs? We compared the diffusabilities of Gouterman's 4-orbitals and those of MOs with amino acid character (Figure 3a). Gouterman's 4-orbitals are more expansive and delocalized than the other MOs, thereby implying that the protein charge can more easily and homogeneously affect their orbital energies, even though the charged amino acid residues have an outermost distribution in the protein shell. In contrast, since the other MOs have compact and localized characters, the effect of the charges of the protein surface could be relatively small. Furthermore, due to the anionic character of the porphyrin ring,[25] in which the gross net charge is −1.59, the 4-orbitals would be more sensitive to the charge of the protein shell.

This expandable property of the 4-orbitals can be explained by the highly ordered polarizability of the porphyrin π or π* nature. Since the unoccupied 4-orbitals correspond to a porphyrin π* orbital derived from the $e_g$ orbital of metalloporphyrins with $D_{4h}$ symmetry having quadratic function ($xz$, $yz$),[22] they can be easily mixed with MOs of the protein shell and thus its effect can be homogeneously expanded into the whole molecule (Figure 4). In the occupied 4-orbitals, a similar expansion effect could be realized: by mixing the porphyrin π orbital derived from $a_{1u}$ and $a_{2u}$ orbitals not having quadratic functions[22] with zinc–sulfur (π) hybridized by sulfur $p_x$ or $p_y$ and zinc $d_{xz}$ or $d_{yz}$, they can acquire $xz$, $yz$ characters (Figure 4).

Because the band-like structure would be a common feature among various kinds of proteins, the type of semiconductor-like behavior can be mostly described by the energy level relationship between the redox center and the protein scaffold. On the other hand, Beratan and co-workers used a donor–acceptor (D–A) coupling indicator, $|H_{fi}|^2$, to

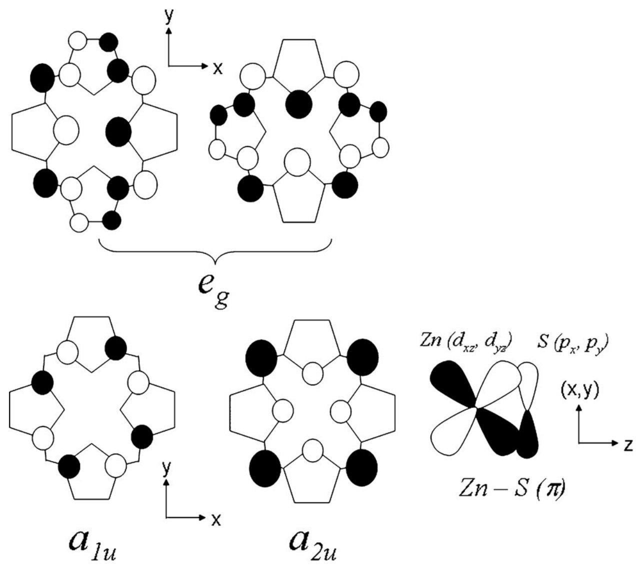


***Figure 4.*** The π-electron densities of Gouterman's 4-orbitals derived from $D_{4h}$ symmetry and Zn–S π-bonding nature. White and black circles are positive and negative aspects, respectively, and the areas are proportional to the π-electron densities.

analyze ET in nine ruthenized cyt $b_{562}$, in which they found a multiple edge-coupling regime and a dominant pathway regime.[26,27] What we have found here is that ET pathways can be more precisely described by the combination of the energy-level relationship and D–A coupling between the responsible MOs [Eq. (1)], that is, analyses of ET rates on the basis of Fermi's Golden Rule by using all-electron wave functions of the protein. Besides the MO coupling term ($H_{fi}$), the proximity in the energy levels [$\delta(E_{fi})$] of donor and acceptor should be tuned for effective electron pathway(s) in the ET protein.

In summary, we have shown that two zinc-substituted cytochromes employ different photoinduced ET mechanisms. The effect of charge on the protein scaffold on the energy of Gouterman's 4-orbitals determines the semiconductor property (n- or p-type) of Zn-cyt $b_{562}$ and Zn-cyt $c$. The energy shift of the 4-orbitals is highly sensitive to changes in the pI because of the expandable and delocalized nature of the MO electron density, most likely because of the highly ordered polarizability of the porphyrin π or π* orbitals. We suggest that a protein semiconductor with a p–n junction could be constructed by fusing two suitably engineered cytochromes.

## Experimental Section

Photocurrent measurements of Zn-cyt $b_{562}$: Photocurrent measurements were carried out using the same system as for previous Zn-cyt $c$ gold electrode measurements.[13] A xenon lamp (Ushio SX-UI150XQ) was used as light source, and monochromated incident light with full width at half maximum of 10 nm was generated by a monochromator (JASCO CT-151T). The incident light was blocked intermittently by a mechanical shutter and focused on the Zn-cyt $b_{562}$ gold electrode in a quartz electrochemical cell (10 mM phosphate buffer solution; counter electrode: Pt mesh; reference electrode: Ag | AgCl). A potentiostat (Hokuto Denko HA150G) was used to control the bias voltage applied to the Zn-cyt $b_{562}$ gold electrode against the reference electrode, and the time course of the current was recorded. All measurements were carried out under nitrogen after 15 min nitrogen bubbling of 10 mM sodium phosphate buffer solution.

Received: May 16, 2011
Revised: September 2, 2011
Published online: October 13, 2011

**Keywords:** cytochromes · density functional theory · electron transfer · hole transfer · protein engineering

[1] I. Bertini, H. B. Gray, E. I. Stiefel, J. S. Valentine, *Biological Inorganic Chemistry: Structure and Reactivity*, University Science Books, Mill Valley, **2006**.
[2] J. L. Dempsey, J. R. Winkler, H. B. Gray, *Chem. Rev.* **2010**, *110*, 7024–7039.
[3] I. Willner, E. Katz, *Bioelectronics: From Theory to Applications*, Wiley-VCH, Weinheim, **2005**.
[4] O. S. Wenger, B. S. Leigh, R. M. Villahermosa, H. B. Gray, J. R. Winkler, *Science* **2005**, *307*, 99–102.
[5] J. N. Onuchic, D. N. Beratan, J. R. Winkler, H. B. Gray, *Annu. Rev. Biophys. Biomol. Struct.* **1992**, *21*, 349–377.
[6] H. B. Gray, J. R. Winkler, *Biochim. Biophys. Acta Bioenerg.* **2010**, *1797*, 1563–1572.
[7] H. B. Gray, J. R. Winkler, *Chem. Phys. Lett.* **2009**, *483*, 1–9.
[8] H. B. Gray, J. R. Winkler, *Q. Rev. Biophys.* **2003**, *36*, 341–372.
[9] R. Langen, I.-J. Chang, J. P. Germanas, J. H. Richards, J. R. Winkler, H. B. Gray, *Science* **1995**, *268*, 1733–1735.
[10] D. V. Vyalikh, A. Kirchner, A. Kade, S. Danzenbächer, Yu. S. Dedkov, M. Mertig, S. L. Molodtsovet, *J. Phys. Condens. Matter* **2006**, *18*, S131–S144.
[11] C. C. Moser, J. L. Anderson, P. L. Dutton, *Biochim. Biophys. Acta Bioenerg.* **2010**, *1797*, 1573–1586.
[12] C. C. Page, C. C. Moser, X. Chen, P. L. Dutton, *Nature* **1999**, *402*, 47–52.
[13] a) Y. Tokita, J. Shimura, H. Nakajima, Y. Goto, Y. Watanabe, *J. Am. Chem. Soc.* **2008**, *130*, 5302–5310; b) Y. Tokita, J. Shimura, H. Nakajima, Y. Goto, Y. Watanabe, *J. Am. Chem. Soc.* **2011**, *133*, 164–165.
[14] A cyt $b_{562}$/$H_2N$-SAM/Au electrode made in the same way as the Zn-cyt $b_{562}$/$H_2N$-SAM/Au electrode showed an adsorbed-type reversible cyclic voltammetric response around 0 V (vs. Ag | AgCl), strongly indicating that the heme side of cyt $b_{562}$ faces the interface (see the Supporting Information, Figure S1). The adsorbed condition of Zn-cyt $b_{562}$ on the $H_2N$-SAM/Au should be the same as that of cyt $b_{562}$.
[15] L. H. Guo, S. Mukamel, G. Mclendon, *J. Am. Chem. Soc.* **1995**, *117*, 546–547.
[16] E. Topoglidis, C. J. Campbell, E. Palomares, J. R. Durrant, *Chem. Commun.* **2002**, 1518–1519.
[17] H. Imahori, H. Norieda, H. Yamada, Y. Nishimura, I. Yamazaki, Y. Sakata, S. Fukuzumi, *J. Am. Chem. Soc.* **2001**, *123*, 100–110.
[18] ET reaction between two molecules is governed by the activation free energy of the Marcus theory, $\Delta G_R^* = (\Lambda/4)(1+\Delta G_0/\Lambda)^2$, where $\Lambda$ is a constant and $\Delta G_0$ corresponds to the redox potential difference between two molecules. In this case, since the redox potential of the photoexcited electron of Zn-cyt $b_{562}$ can approximate the energy of the unoccupied 4-orbitals, $\Delta G_0$ in methyl viologen is smaller than that in potassium ferricyanide, which suggests that the cathodic photocurrent of Zn-cyt $b_{562}$ was enhanced by methyl viologen but not potassium ferricyanide. Photocurrents have also been obtained from the Au/SAM/Zn-cyt $b_{562}$ electrode even though there was no methyl viologen in the solution. Since the electron acceptor is not clear, we need to clarify it in the future.
[19] M. D. Newton, *Chem. Rev.* **1991**, *91*, 767–792.
[20] F. Sato, T. Yoshihiro, M. Era, H. Kashiwagi, *Chem. Phys. Lett.* **2001**, *341*, 645–651.
[21] R. G. Parr, W. Yang, *Density-Functional Theory of Atoms and Molecules*, Oxford University Press, New York, **1995**.
[22] D. Dolphin, *The Porphyrin*, Academic Press, New York, **1977**.
[23] $H_{fi}$ corresponds to the $F'$ matrix of the Hartree–Fock theory calculated from unitary conversion of the final Fock matrix of the Kohn–Sham–Roothaan equation and $\delta(E_{fi})$ is the delta function of the energy difference between effective final and initial MOs.
[24] A. Kuki, P. G. Wolynes, *Science* **1987**, *236*, 1647–1652.
[25] T. Miyahara, Y. Tokita, H. Nakatsuji, *J. Phys. Chem. B* **2001**, *105*, 7341–7352.
[26] T. R. Prytkova, I. V. Kurnikov, D. N. Beratan, *Science* **2007**, *315*, 622–625.
[27] In the present case with Zn-cyt $b_{562}$, ET within the conduction band is more plausible. In the work by Prytkova et al., ET from $Fe^{II}$ to $Ru^{III}$ in the ruthenized cyt $b_{562}$ has been examined, and HT within the valence band of proteins is responsible. This can also be explained by the energy-level relationship between the protein's band structure and redox centers. The two redox centers, Ru and Fe complexes with higher redox potentials ($E_{0Ru^{II}/Ru^{III}}$ =0.8 V, $E_{0Fe^{II}/Fe^{III}}$ =0.05 V vs. Ag | AgCl), preferentially interact through the valence band of the protein scaffold, namely the HT mechanism.

  